Inorganic Chemistry

Article

pubs.acs.org/IC

Synthesis and Structural Elucidation of Triazolylmolybdenum(VI) Oxide Hybrids and Their Behavior as Oxidation Catalysts

Andrey B. Lysenko,*[,†] Ganna A. Senchyk,[†] Konstantin V. Domasevitch,[†] Jürg Hauser,[‡] Daniel Fuhrmann,[§] Merten Kobalz,[§] Harald Krautscheid,[§] Patrícia Neves,[∥] Anabela A. Valente,[∥] and Isabel S. Gonçalves*[,∥]

[†]Inorganic Chemistry Department, Taras Shevchenko National University of Kyiv, Volodimirska Street 64, Kyiv 01033, Ukraine

[‡]Departement für Chemie und Biochemie, Universität Bern, Freiestrasse 3, CH-3012 Bern, Switzerland

[§]Institut für Anorganische Chemie, Universität Leipzig, Johannisallee 29, D-04103 Leipzig, Germany

[∥]Department of Chemistry, CICECO - Aveiro Institute of Materials, University of Aveiro, Campus Universitário de Santiago, 3810-193 Aveiro, Portugal

Supporting Information

ABSTRACT: A large family of bifunctional 1,2,4-triazole molecular tectons (tr) has been explored for engineering molybdenum(VI) oxide hybrid solids. Specifically, tr ligands bearing auxiliary basic or acidic groups were of the type amine, pyrazole, 1*H*-tetrazole, and 1,2,4-triazole. The organically templated molybdenum(VI) oxide solids with the general compositions $[MoO_3(tr)]$, $[Mo_2O_6(tr)]$, and $[Mo_2O_6(tr)(H_2O)_2]$ were prepared under mild hydrothermal conditions or by refluxing in water. Their crystal structures consist of zigzag chains, ribbons, or helixes of alternating *cis*-$\{MoO_4N_2\}$ or $\{MoO_5N\}$ polyhedra stapled by short [N−N]-tr bridges that for bitriazole ligands convert the motifs into 2D or 3D frameworks. The high thermal (235−350 °C) and chemical stability observed for the materials makes them promising for catalytic applications. The molybdenum(VI) oxide hybrids were successfully explored as versatile oxidation catalysts with *tert*-butyl hydroperoxide (TBHP) or aqueous H_2O_2 as an oxygen source, at 70 °C. Catalytic performances were influenced by the different acidic−basic properties and steric hindrances of coordinating organic ligands as well as the structural dimensionality of the hybrid.

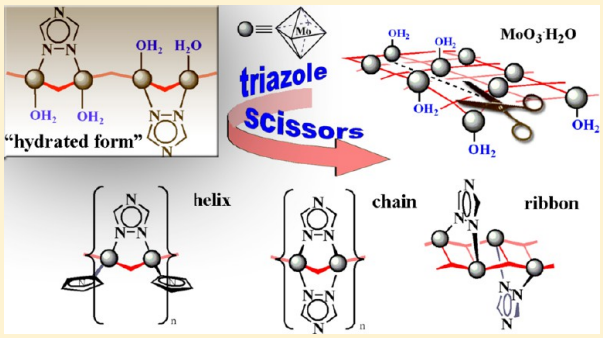

INTRODUCTION

Metal oxide−organic solids will always be the central focus of highly topical interdisciplinary areas of materials chemistry.[1] In one particular application, the development of solid catalysts that promote oxygen transfer to olefins, giving epoxides, is important for organic chemistry and the chemical industry.[2,3] Among numerous candidates studied for this purpose,[2,3] organic−inorganic materials based on polyoxomolybdates have proven to be one of the most promising classes of hybrids.[4−6] On the one hand, these species, typically consisting of linked molybdenum oxide polyhedra with a bridging μ_{2-4}-O oxide, terminal Mo═O molybdenyl units, and organic ligands directly bonded to the Mo centers, are very prone to react with peroxides, leading to reactive intermediates like oxodiperoxomolybdenum $[MoO(O_2)_2]$.[2,6] On the other hand, the compounds combine several valuable advantages: sufficient thermal (~200−400 °C) and chemical stability as well as high catalytic activity and selectivity. The employment of organic building blocks with *N*-heteryl and carboxylic acid donor groups offers a lot of latitude for modifying the structure of the molybdenum(VI) oxide matrix, thus allowing tuning of the desired properties. For instance, a few of the organically modified MoO_3 hybrids $\{(Himi)_4[(imi)_2(Mo_8O_{26})]\cdot H_2O$, with imi = *N*,*N*′-butylenediimidazole,[5a] $[MoO_3(2,2'\text{-bipy})]$-$[MoO_3(H_2O)]$,[5b] $[Mo_3O_9(pzpy)]$,[5c] with pzpy = 2-[3(5)-pyrazolyl]pyridine, etc.} demonstrated high catalytic efficiency in olefin epoxidation in the presence of various oxidants. Very recently, the ligand design concept was successfully applied toward the synthesis of a family of hybrid organic−inorganic semiconductors $MO_3(L)$ ($M = Mo^{VI}$ or W^{VI}; L = N,N-chelating or bridging heterocycles), which exhibited broad band-gap tunability, negative thermal expansion, reduced thermal conductivity, etc.[7] Apparently, the interaction of layered $MoO_3\cdot nH_2O$ ($WO_3\cdot nH_2O$) with *N*-heteryl ligands can be exploited for the preprogrammed construction of the solids. Thus, chelating 2,2′-bipyridine (2,2′-bipy), 1,10-phenanthroline (1,10-phen), and ethylenediamine (en) preferably yield chain or ribbon oxides constituted by vertex-sharing polyhedra $\{MO_4N_2\}$,[5b−e,7−10] while pyridine and its related bridging analogues like pyrazine and 4,4′-bipy behave as intercalates in the perovskite-type structure.[11−14] Even more interesting is the situation when triazole ligands replace the pyridine derivatives in the reaction systems. Being able to coordinate two metal

Received: May 5, 2015
Published: August 17, 2015

DOI: 10.1021/acs.inorgchem.5b01007
Inorg. Chem. 2015, 54, 8327−8338

sites simultaneously, 1,2,4- and 1,2,3-triazoles furnish new insight into the design concept of metal oxide−organic frameworks (MOOFs).[15] Unexpectedly, the intercalated structure of MoO_3−tr hybrids (type I) shown in Scheme 1 is

Scheme 1. Structural Types of 1,2,4-Triazole-Templated MOOFs (Type I, a Layer Motif; types II and III, Corner-Sharing $\{MoO_4N_2\}$ Chains Supported by Single or Double [N−N]-tr Bridges; type IV, a Ribbon Formed from Two Cross-Linked Chains; Type V, a Novel Chain Motif Containing Coordinated Water Molecules and Bridging tr Units)

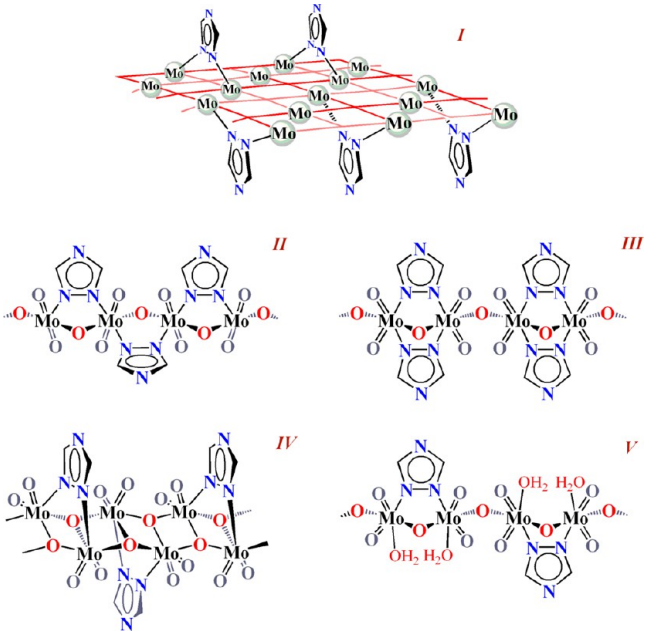

quite rare and was only observed for two complexes, $MoO_3(1H\text{-}1,2,3\text{-tr})_{0.5}$ and $MoO_3(1H\text{-}1,2,4\text{-tr})_{0.5}$.[12b,14] In contrast, 4-substituted 1,2,4-triazole molecules exhibit a clear tendency to form chainlike topological motifs (types II−IV), which differ in the sequence and arrangement of [N−N]-tr bridges.[15] For 1,2,4-bitriazole ligands, the wavy chain, ribbon, or 4_1-helix subtopologies initially formed can be rationally transformed into 2D or 3D frameworks. Indeed, the principle of ligand design, widely employed toward coordination polymers, is also becoming more challenging in the field of MOOFs.

In this paper, we introduce a series of representative ligands bearing 1,2,4-triazole(s) as a primary group and amine, pyrazole, or 1*H*-tetrazole as a secondary group (Scheme 2). The diverse set of functions separated by suitable linkers can specifically influence the resultant MOOF structure, implementing a substantial difference in their acidic−basic properties. The enhancement or weakening of Lewis and Brønsted acidity could result in the tailoring of catalytic properties of the molybdenum oxide hybrid compounds. The synthesis of the solids can be typically achieved under hydrothermal conditions and requires simple techniques for crystal growth, which is a distinct benefit.

EXPERIMENTAL SECTION

Measurements. Elemental analysis was carried out with a Vario EL-Heraeus microanalyzer. IR spectra (400−4000 cm^{-1}) were measured with a PerkinElmer Fourier transform infrared (FT-IR)

Scheme 2. Series of 1,2,4-Triazolyl Derivatives with Extra Functional Groups (Amine, Pyrazole, 1*H*-Tetrazole, and 1,2,4-Triazole)

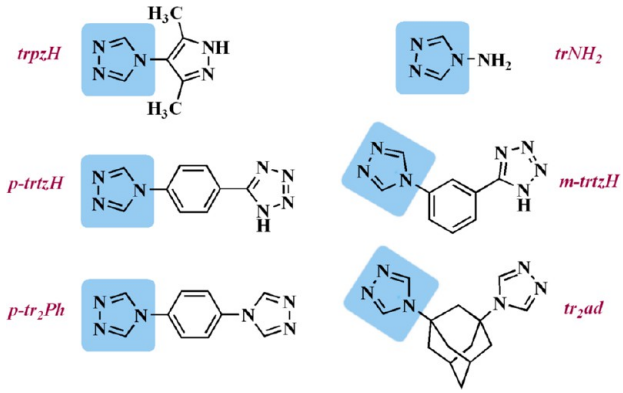

spectrometer (KBr pellets) and with a Mattson 7000 spectrometer, using a globar source, a DTGS detector, and KBr cells, with 2 cm^{-1} resolution and triangular apodization. The room temperature (rt) powder X-ray diffraction (PXRD) patterns were measured using a Stoe STADIP diffractometer (Cu $K\alpha_1$, using a linear PSD detector). The temperature-dependent X-ray measurements were recorded on a Stoe STADIP diffractometer with a high-temperature attachment and an image-plate detector system. Simultaneous thermogravimetric/differential thermal analysis/mass spectrometry (TG/DTA−MS) studies were carried out on a Netzsch F1 Jupiter device connected to an Aeolos mass spectrometer. Samples were heated at a rate of 10 K min^{-1}. Scanning electron microscopy (SEM) images were collected using a Hitachi SU-70 microscope operating at 15 kV.

X-ray Crystallography. The diffraction data were collected with graphite-monochromated Mo Kα radiation (λ = 0.71073 Å) using a Stoe Image Plate Diffraction System (for **1** and **4b−6**, numerical absorption correction using X-RED and X-SHAPE[16]) and a Bruker APEXII CCD area-detector diffractometer (ω scans; for **2** and **3**). The data were corrected for Lorentz−polarization effects and for the effects of absorption (multiscan method). The structures were solved by direct methods and refined by full-matrix least squares on F^2 using the *SHELX-97* package.[17] All atoms, including water O atoms, were refined anisotropically. The OH and NH H atoms were located and then fixed with U_{iso} = 1.5U_{eq}(O,N). The CH H atoms were added geometrically [U_{iso} = 1.2U_{eq}(C)] and refined as riding atoms. For **5**, the H atoms of the solvate water molecule were not located. Crystals of complex **4b** exhibit nonmerohedral twinning, as was indicated by the large fraction of unindexed reflections and parameters of the crystal structure refinement: R1 = 0.13, systematically $F_o^2 \gg F_c^2$, and large residual electron density peaks above 5.0 e $Å^{-3}$. Therefore, the data frames were indexed and integrated as a two-domain system using RECIPE/TWIN facilities implemented in the Stoe IPDS software.[18] The data were scaled and merged, yielding a single data set of 62% completeness due to a partial overlap of the reflections corresponding to different domains of the crystal. Graphical visualization of the structures was made using the program *Diamond 2.1e*.[19]

Crystallographic data and experimental details for structural analyses are summarized in Table S1. The crystallographic material can also be obtained from the Cambridge Crystallographic Data Centre, with deposition numbers CCDC 1061683−1061688 for **1−3**, **4b**, **5**, and **6**, respectively.

Catalytic Tests. Catalytic reactions were carried out at 70 °C in 5 mL borosilicate reactors equipped with valves for sampling and a poly(tetrafluoroethylene) magnetic stirring bar. Typically, an amount of molybdenum coordination polymer equivalent to 18 μmol of molybdenum, 1.8 mmol of substrate, and 2 mL of cosolvent was added to the reactor, which was subsequently immersed in a thermostated oil bath under stirring (1000 rpm). After 10 min, 2.75 mmol of oxidant was added, and this point was considered the initial instant of the catalytic reaction. The tested substrates were *cis*-cyclooctene (Cy; 95%,

DOI: 10.1021/acs.inorgchem.5b01007
Inorg. Chem. 2015, 54, 8327−8338

Aldrich), benzyl alcohol (BzOH; anhydrous, 99.8%, Aldrich), and benzaldehyde (PhCHO; ≥99%, Aldrich). The tested cosolvents were α,α,α-trifluorotoluene (TFT; ≥99%, Aldrich) and CH_3CN (99.9%, Panreac). The oxidants used were *tert*-butyl hydroperoxide in decane (TBHP; ca. 5.5 M, Aldrich) and aqueous H_2O_2 (30 wt %, Aldrich).

Evolution of the catalytic reactions was monitored by gas chromatography (GC). For reactions with H_2O_2, individual experiments were performed for a given reaction time. Prior to sampling, the reactors were cooled to ambient temperature. The samples were analyzed using a Varian 3900 gas chromatograph equipped with a DB-5 capillary column (30 m × 0.25 mm × 0.25 μm), a flame ionization detector, and dihydrogen as the carrier gas. Identification of the reaction products was carried out by GC−MS [GC-qMS Agilent Technologies, 6890 N Network GC system, 5973 Network mass-selective detector, equipped with a DB-1 capillary column (30 m × 0.25 mm × 0.10 μm)] using helium as the carrier gas. Undecane and nonane were used as internal standards added after reaction for the Cy and BzOH/PhCHO systems, respectively.

In order to investigate the nature of active species formed during catalytic reactions, after a catalytic batch run, the solid phase (when present) was separated from the reaction mixture by centrifugation (3500 rpm), thoroughly washed with pentane or ethanol, and dried under vacuum, at 60 °C for 1 h. From the liquid phase, metal species were isolated by the addition of a diethyl ether/pentane mixture to the solution (which was previously filtered using a 0.2 μm nylon membrane), followed by storage at 4 °C overnight. The precipitated solid was separated by centrifugation, washed with acetone, and dried in a fashion similar to that described above for the undissolved solids. All recovered solids were characterized by FT-IR attenuated total reflectance (ATR) and PXRD for comparison with the corresponding original compounds.

A contact test (ct) was carried out for compound **2** with TBHP as the oxidant, as follows. The compound was treated under conditions similar to those used for a typical batch run with TBHP/TFT, but without a substrate, for 24 h at 70 °C. The resultant biphasic solid−liquid mixture was cooled to ambient temperature and centrifuged (3500 rpm) to separate the solid and liquid phases. The liquid phase (L) was passed through a filter equipped with a 0.2 μm nylon membrane, giving **2**-L-ct, and used for the (homogeneous catalytic) reaction of Cy with TBHP; for this purpose, Cy was added to the liquid to give an initial substrate concentration of 0.7 M, and this solution was stirred for 24 h at 70 °C. The solid obtained from the ct was recovered in a fashion similar to that described above for catalyst reuse, giving **2**-S-ct, which was characterized by FT-IR ATR and PXRD. Subsequently, the solid **2**-S-ct was tested as the catalyst for the reaction of Cy with TBHP, at 70 °C (the initial mass ratios of the olefin/oxidant/metal compound were the same as those used for the typical reaction conditions). After a 24 h catalytic batch run using **2**-S-ct, a biphasic solid−liquid mixture was obtained. The solid was recovered in a fashion similar to that described above for catalyst reuse, giving (**2**-S-ct)-run1, which was subsequently characterized by FT-IR ATR and PXRD for comparison with the original compound **2**.

Caution! *Hydrofluoric acid (HF) is toxic and corrosive, even if a diluted aqueous solution is used, and must be handled in a well-ventilated fume hood with extreme caution using appropriate protective gear.*

Synthesis of the Coordination Compounds. All chemicals were of reagent grade and were used as received without further purification. 4-Amino-1,2,4-triazole ($trNH_2$; commercial), 4-(3,5-dimethyl-1*H*-pyrazol-4-yl)-1,2,4-triazole (trpzH), 5-[4-(1,2,4-triazol-4-ylphenyl)]-1*H*-tetrazole (*p*-trtzH), 5-[3-(1,2,4-triazol-4-ylphenyl)]-1*H*-tetrazole (*m*-trtzH), 1,4-phenylene-4,4′-bis(1,2,4-triazole) (*p*-tr_2Ph), and 1,3-bis(1,2,4-triazol-4-yl)adamantane (tr_2ad) were prepared according to previously described procedures.[20]

[MoO_3(trNH$_2$)] ***(1)***. MoO_3 (180 mg, 1.25 mmol) was dissolved in refluxing water (220 mL) under continuous stirring for a few hours. To the solution was added $trNH_2$ (105 mg, 1.25 mmol), and refluxing was continued for another 1 h. The resultant colorless solution was cooled to rt, leading to a white precipitate. This solid was filtered off, washed with water and CH_3OH, and dried in an oven at 70 °C for 1 h, affording 245 mg of the desired product (yield 86%). Anal. Calcd for $C_2H_4MoN_4O_3$: C, 10.53; H, 1.77; N, 24.57. Found: C, 10.39; H, 1.85; N, 24.32. The rt PXRD pattern of the product was identical with that of the monocrystalline sample prepared as follows.

Single crystals suitable for X-ray analysis were synthesized in the hydrothermal reaction between 4,4′-bis(1,2,4-triazole) (27.2 mg, 0.200 mmol) and MoO_3 (14.3 mg, 0.0994 mmol) in 3 mL of water using a 20 mL Teflon-lined autoclave. The mixture was heated to 140 °C, held there for 24 h, and then slowly cooled to rt for 48 h. The resultant deep-blue solution contained colorless needles of the product (∼4.0 mg), which were collected by filtration, washed with water, and dried. Because of its low thermal stability, 4,4′-bis(1,2,4-triazole) serves as a source of $trNH_2$.

[Mo_2O_6(trpzH)(H_2O)$_2$] ***(2)***. MoO_3 (179 mg, 1.24 mmol) was dissolved in refluxing water (160 mL) under continuous stirring. To the solution was added trpzH (102 mg, 0.625 mmol), and refluxing was continued for an additional 5 h. Cooling to rt afforded a white cotton-like precipitate of the product (250 mg, 83%). Anal. Calcd for $C_7H_{13}Mo_2N_5O_8$: C, 17.26; H, 2.69; N, 14.38. Found: C, 17.37; H, 2.79; N, 14.32.

Monocrystalline sample **2** was prepared under hydrothermal conditions starting from MoO_3 (32.6 mg, 0.226 mmol) and trpzH (28.6 mg, 0.175 mmol) in 10 mL of water using a 20 mL Teflon-lined autoclave. The mixture was heated to 165 °C, held there for 12 h, and then cooled to rt for 48 h. The resultant colorless needles of the product were collected by filtration, washed with water, and dried (yield: 40.1 mg, 73%).

[Mo_2O_6(m-trtzH)(H_2O)$_2$] ***(3)***. A mixture of MoO_3 (30.0 mg, 0.208 mmol), *m*-trtzH (21.5 mg, 0.101 mmol), water (10 mL), and a 7% aqueous solution of HF (50 μL) as a mineralizing agent was sealed in a 20 mL Teflon-lined autoclave. The autoclave was heated to 140 °C, held there for 24 h, and then cooled to rt for 48 h. The resultant mixture containing the desired complex as a major product as well as starting materials MoO_3 and *m*-trtzH as minor impurities was filtered off, dried, and ground using a mortar and pestle. Similar to a previously described method,[21] a $CHCl_3$/$CHBr_3$ solvent mixture was then used for the density separation of compound **3**. The white crystalline solid was washed with CH_3OH and dried at rt (yield: 28.3 mg, 52%). Anal. Calcd for $C_9H_{11}Mo_2N_7O_8$: C, 20.13; H, 2.06; N, 18.25. Found: C, 20.08; H, 2.11; N, 18.19.

[MoO_3(p-trtzH)] ***(4a)***. Complex **4a** was described and structurally characterized by us earlier.[15] Herein we further optimized the synthesis. A mixture of MoO_3 (30.0 mg, 0.208 mmol), *p*-trtzH (21.5 mg, 0.101 mmol), water (10 mL), and a 7% aqueous solution of HF (100 μL) as a mineralizing agent was sealed in a 20 mL Teflon-lined autoclave. The autoclave was heated using the same temperature regime as that described for **3**. The resultant crystalline mixture contained the desired complex as a major product as well as unreacted starting materials MoO_3 and *m*-trtzH as minor impurities. The solids were filtered off, dried, and ground using a mortar and pestle. A $CHCl_3$/$CHBr_3$ solvent mixture was used for the density separation of complex **4a**. The white crystalline solid was washed with CH_3OH and dried at rt (yield: 20.1 mg, 55%). Anal. Calcd for $C_9H_7MoN_7O_3$: C, 30.27; H, 1.98; N, 27.45. Found: C, 30.22; H, 2.00; N, 27.42.

Thin needles of complex [Mo_2O_6(*p*-trtzH)] (**4b**) were isolated in very low yield (∼1%) under identical conditions without the addition of HF. Anal. Calcd for $C_9H_7Mo_2N_7O_6$: C, 21.57; H, 1.41; N, 18.19. Found: C, 21.50; H, 1.47; N, 18.11.

[Mo_2O_6(p-tr_2Ph)] ***(5)***. *p*-tr_2Ph (21.5 mg, 0.101 mmol), $(NH_4)_6Mo_7O_{24}{\cdot}4H_2O$ (45.0 mg, 36.4 μmol), and 10 mL of water were sealed in a 20 mL Teflon-lined autoclave. The autoclave was heated to 140 °C, held there for 24 h, and slowly cooled to rt for 48 h. The resultant crystalline mixture contained the desired complex as a major product and unreacted *p*-tr_2Ph as a minor impurity. The solids were filtered off, dried, and ground. Similar to the synthesis of compounds **3** and **4a**, a $CHCl_3$/$CHBr_3$ solvent mixture was used for the density separation of complex **5**. The white crystalline solid was washed with CH_3OH and Et_2O and dried at rt (yield: 39.0 mg, 77%). Anal. Calcd for $C_{10}H_8Mo_2N_6O_6$: C, 24.02; H, 1.61; N, 16.81. Found: C, 24.00; H, 1.64; N, 16.79.

DOI: 10.1021/acs.inorgchem.5b01007
Inorg. Chem. 2015, 54, 8327−8338

The isolation procedure using organic solvents yielded the dehydrated product **5**, according to elemental analysis and thermogravimetric analysis (TGA) data. However, single crystals of the compound agreed with the formula $[Mo_2O_6(p\text{-}tr_2Ph)]\cdot H_2O$. Anal. Calcd for $C_{10}H_{10}Mo_2N_6O_7$: C, 23.18; H, 1.95; N, 16.22. Found: C, 23.11; H, 2.00; N, 16.12.

*$[Mo_2O_6(tr_2ad)]\cdot H_2O$ (**6**).* tr_2ad (27.0 mg, 99.9 μmol) and $(NH_4)_6Mo_7O_{24}\cdot 4H_2O$ (35.3 mg, 28.6 μmol) in 5 mL of water were placed in a 20 mL Teflon-lined autoclave before being sealed. The autoclave was heated to 160 °C, held there for 20 h, and slowly cooled to rt for 44 h. The monophasic product formed was isolated as colorless blocks in a 45.0 mg yield (78%). Anal. Calcd for $C_{14}H_{20}Mo_2N_6O_7$: C, 29.18; H, 3.50; N, 14.58. Found: C, 29.13; H, 3.61; N, 14.51.

RESULTS AND DISCUSSION

Synthesis and Crystal Structures. In the proposed series of 1,2,4-triazole-based tectons (Scheme 2), the extra functional groups (amine, pyrazole, or 1*H*-tetrazole) are responsible for achieving the appropriate acid–base characteristics. The available aromatic, aliphatic, or C–N spacers provide semirigid geometric dispositions between multiple N-donor centers. The key role of the 1,2,4-triazole group is an entry point in the following discussion. Thus, a prime interaction between triazoles and a molybdenum(VI) oxide matrix can be rationalized, as displayed in Scheme 3. First, two-point [N–N]-tr anchors facilitate the high-temperature depolymerization of β-$MoO_3\cdot H_2O$ with the further reverse formation of chain structural variations upon hydrothermal crystallization. The structure of layered MoO_3(1*H*-1,2,4-triazole)$_{0.5}$ is just the exception that proves the rule.[12b] In the latter case, the behavior of 1*H*-1,2,4-triazole resembles that of pyridine, pyrazine, or their bridging derivatives, resulting in the pillared-layered MoO_3 hybrids. The formation of more common chainlike motifs, shown in Scheme 3, can be explained by assuming that the presented "hydrated form" is an important intermediate structure. This provides a better understanding of the structural interplay in the systems. It can be easily imagined that a "ribbon type" is a self-condensation product of two "hydrated chains". The other isomeric pair of chains is also derived from the "hydrated form" by successive substitution of coordinating water molecules with triazole ligands. To the best of our knowledge, this structural precedent was not described earlier.

Scheme 3. Structural Relationship between Triazole–Molybdenum(VI) Oxide Hybrids

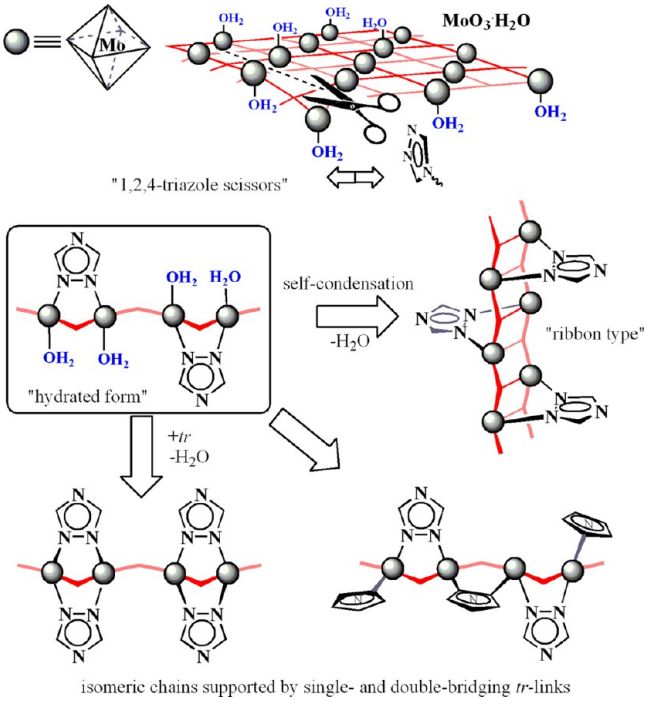

Because four organic ligands, *m*-trtzH, *p*-trtzH, *p*-tr_2Ph, and tr_2ad, were found to be poorly soluble in water, the preparation of their molybdenum(VI) oxide complexes under hydrothermal conditions was particularly desirable. At the initial step, it also allowed us to isolate single crystals of a few key compounds and to elucidate their structures employing X-ray diffraction analysis (Table 1). Fortunately, for a couple of water-soluble ligands, trpzH and $trNH_2$, the self-assembly proceeded in aqueous solutions of MoO_3 (5.7–7.8 mM) under simple refluxing. These experiments, performed on a relatively large scale (~250 mg), afforded **1** and **2** as cotton-like precipitates in high yield (>80%).

The crystal structures of two related compounds, **2** and **3**, belong to the "hydrated type" mentioned above, in which molybdenum octahedra {$MoNO_5$} form a sinusoidal wire (Figure 1a,b). The triazole groups coordinate to the corner-sharing Mo centers in the expected μ_2 fashion, thereby supporting an inorganic chain construction.

Despite significant differences between the pK_A values of dimethylpyrazole (pK_a ~ 9.0) and 1*H*-tetrazole (pK_a ~ 4.9), both termini appear in uncharged forms, which are involved in a rich set of intermolecular hydrogen bonding (Figures S4 and S6). For the amphoteric ligands, trpzH and *m*-trtzH, the reaction products of the hydrothermal synthesis are determined by the acidic–basic properties of the medium, which, in a typical experiment, was slightly acidic (pH ~ 4–5). Being more basic than 1,2,4-triazole (pK_b ~ 2.39),[22] the dimethylpyrazole fragment (pK_b ~ 9.74) demonstrates a weaker coordination ability toward Mo^{VI} ions. Probably, in this particular case, the steric bulk of two methyl groups of dimethylpyrazole exerts a more important role that dominates over its basic properties.

Another ligand *p*-trtzH containing tetrazole termini in the para position of the phenylene linker possesses almost identical acidic–basic properties to those of its meta isomer. Complexes with similar structures could, therefore, be formed, but in reality this is not the case. The discrimination between the structural types of **3**, **4b** (a minor phase, see the details in the Experimental Section), and the previously described **4a**[15] (4_1-helical chain, a dominating phase) is more distinct. The crystal structure of **4b** consists of a double chain of edge-sharing molybdenum oxide distorted octahedra that are stabilized by [N–N]-tr links in an up-and-down mode (Figure 2a). A similar MoO_3 ribbon motif supported by some heteryl carboxylates was earlier described.[23] In these complexes, the deprotonated carboxylic function serves as a syn,syn-μ_2-η^1:η^1 bridge between Mo atoms, indicating the close relationship between carboxylate and triazole.

Although the acidic–basic properties and the sizes of *p*-trtzH and $trNH_2$ are markedly different, the crystal structures of their two complexes, **4a**[15] and **1**, are closely related. The molybdenum *cis*-{N_2O_4} octahedra share common vertexes from μ_2-O atoms, leading to 4_1-helical chains [MoO_3([N–N]-tr)] (Figure 2b; structural type II). Within the chains, the triazole groups additionally "staple" the neighboring polyhedra through two closest vertexes. The auxiliary amino and tetrazole

DOI: 10.1021/acs.inorgchem.5b01007
Inorg. Chem. 2015, 54, 8327–8338

Table 1. Some Structural and Geometric Features Observed in the Crystal Structures of 1−6 (Å)

compound	coordination environment of Mo	polyhedral connectivity	topology and molybdenum(VI) oxide subtopology	coordination motif; see Scheme 1
$[MoO_3(trNH_2)]$ (**1**)	*cis*-$\{N_2O_4\}$	corner-shared	1D, 4_1 helix	type II
$[Mo_2O_6(trpzH)(H_2O)_2]$ (**2**)	$\{NO_5\}$	corner-shared	1D, chain	type V
$[Mo_2O_6(m\text{-}trtzH)(H_2O)_2]$ (**3**)	$\{NO_5\}$	corner-shared	1D, chain	type V
$[MoO_3(p\text{-}trtzH)]$ (**4a**)[15]	*cis*-$\{N_2O_4\}$	corner-shared	1D, 4_1 helix	type II
$[Mo_2O_6(p\text{-}trtzH)]$ (**4b**)	$\{NO_5\}$	corner- and edge-shared	1D, ribbon	type IV
$[Mo_2O_6(p\text{-}tr_2Ph)]\cdot H_2O$ (**5**)	*cis*-$\{N_2O_4\}$	corner-shared	3D, 4_1 helix	type II
$[Mo_2O_6(tr_2ad)]\cdot H_2O$ (**6**)	*cis*-$\{N_2O_4\}$	corner-shared	2D layer, chain	type III

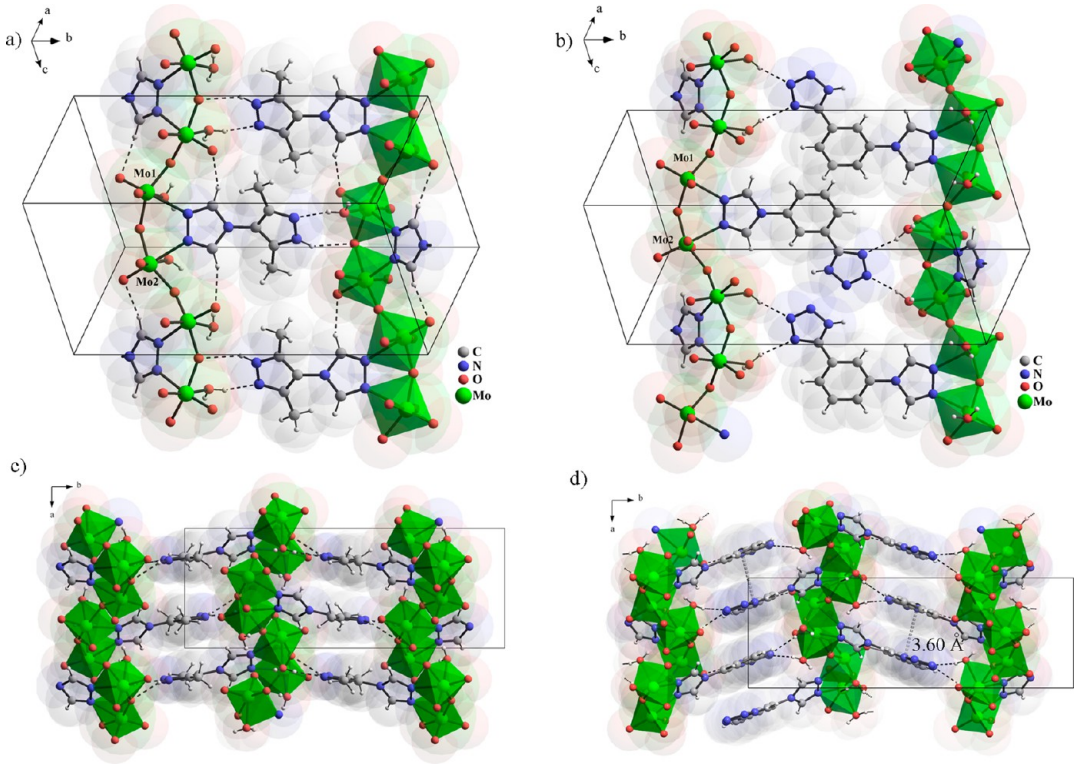

Figure 1. Two complexes, **2** (a and c) and **3** (b and d), belonging to a new "hydrated form" (type V; please also see Table 1) containing water molecules directly coordinated to Mo centers.

functions serve as hydrogen-bonding donor/acceptor modules for the interconnection of adjacent helixes of opposite chirality.

The principle structural changes for triazole−molybdenum oxide hybrids were achieved by introducing the second triazole moiety (*p*-tr_2Ph and tr_2ad). Apparently, the crystal structure of the solids can be rationalized because the formation of $[MoO_3([N{-}N]\text{-}tr)]_n$ linear motifs seems to be very predictable. For a family of bitriazoles, this can afford more complex construction depending on the geometrical and conformational features of the ligand. Thus, the reaction of linear *p*-phenylene-bridged bis(1,2,4-triazole) (*p*-tr_2Ph) and molybdenum(VI) oxide resulted in a 3D framework structure of **5**·H_2O (Figure 3). The well-recognizable helical chains are built up from *cis*-$\{MoN_2O_4\}$ octahedra and belong to the structural type II (Table 1). The bitriazole ligands act exclusively as tetradentate tectons linking a pair of Mo atoms along the chain as well as interconnecting the neighboring chains in tetragonal packing. The porosity of such an arranged framework is eliminated by the interpenetration of two identical nets (Figure 3c), leaving the minimal volume to accommodate water molecules in the lattice.

The angular module tr_2ad, in which two triazole groups are attached to a bulk adamantane scaffold, also offers the possibility of a 3D microporous framework. However, in our hands, the hydrothermal reaction of tr_2ad and molybdenum(VI) oxide usually led to a mixture of unidentified products. We found that the use of $(NH_4)_6Mo_7O_{24}\cdot 4H_2O$, taken as a molybdenum(VI) source, afforded an exclusive formation of a new crystalline phase of **6**·H_2O. The crystal structure of **6** contains sinusoidal chains of molybdenum oxide. Each pair of *cis*-$\{MoN_2O_4\}$ octahedra is joined by a common vertex of a μ_2-O atom and by a short [N−N]-tr "clamp". The angular disposition of triazole groups around the adamantane spacer causes an interconnection of the neighboring MoO_3 chains in extended layers (Figure 4). As a consequence, the organic ligands are successively distributed along the *ac* plane above and below the layer, forming small channels with a dimension of 1.5 × 1.5 Å along the *a* axis. The solvate water molecules

DOI: 10.1021/acs.inorgchem.5b01007
Inorg. Chem. 2015, 54, 8327−8338

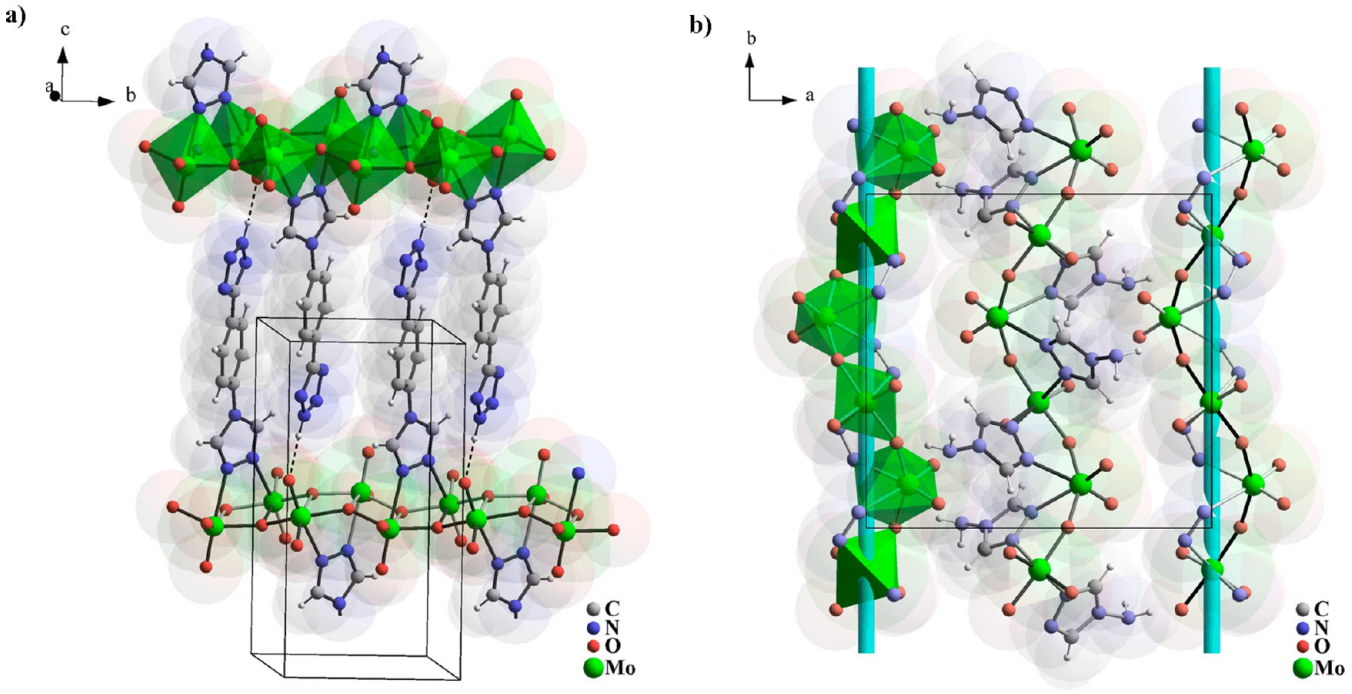

Figure 2. (a) Ribbon-type complex **4b** prepared as a minor phase. The phenylene and tetrazole groups within one *p*-trtzH molecule are positioned nearly coplanar, but they both are noncoplanar to the triazole termini. The almost flat tzH−ph fragments of two neighboring ribbons, a result of intermolecular π-stacking interactions, are fastened to one another like sequentially spaced blades, stabilized by N−H···O bonding interactions. (b) 4_1-helical structural motif in **1** stapled by [N−N]-triazole "clamps".

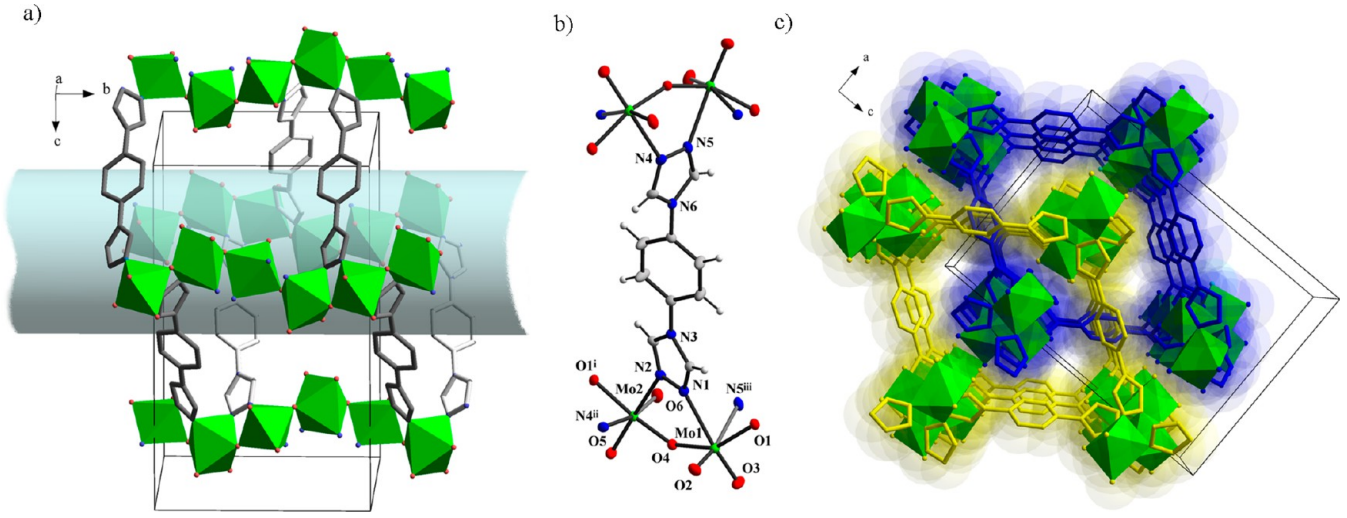

Figure 3. Structure of **5**·H_2O. Symmetry codes: (i) $1 - x, -0.5 + y, 0.5 - z$, (ii) $0.5 + x, 0.5 - y, 1 - z$, (iii) $0.5 - x, 1 - y, -0.5 + z$. Two independent tetragonally arranged frameworks (wire mode) interpenetrating to exclude the microporous behavior. Small channels house crystallization water (not shown); Mo atoms are shown as polyhedra.

reside close to molybdenyl O atoms and are trapped in the cages by means of tight interlayer packing.

Thermal Stability. A combination of temperature-dependent PXRD and thermogravimetry/mass spectrometry (TG-MS) was applied for a clear understanding of thermal decomposition and phase transformation processes. The latter were recently observed for many triazolyl-supported metal−organic frameworks (MOFs) and MOOFs.[15,24,25]

As follows from Table 2 (please also see Figures S22−S27), the molybdenum oxide hybrids possess sufficient thermal stability. Two related complexes, **2** and **3**, containing coordinated aqua ligands undergo primarily dehydration above 115 and 150 °C (m/z 18), followed by final MOOF decompositions above 280 and 235 °C (m/z 44; CO_2), respectively. For complexes **6** and **1** with uncoordinated and surface-adsorbed water molecules, the dehydration processes proceed similarly in the same temperature range. In contrast, a crystalline sample of **5**·H_2O readily lost the crystallization water at rt during a purification procedure (see the Experimental Section). This, however, did not afford any structural changes. Upon heating of compound **2**, the crystal structure showed a two-step transformation before undergoing collapse (Figure 5). The point was clearly evidenced by PXRD patterns measured at different temperatures (Figure S23). The main diffraction peaks

DOI: 10.1021/acs.inorgchem.5b01007
Inorg. Chem. 2015, 54, 8327−8338

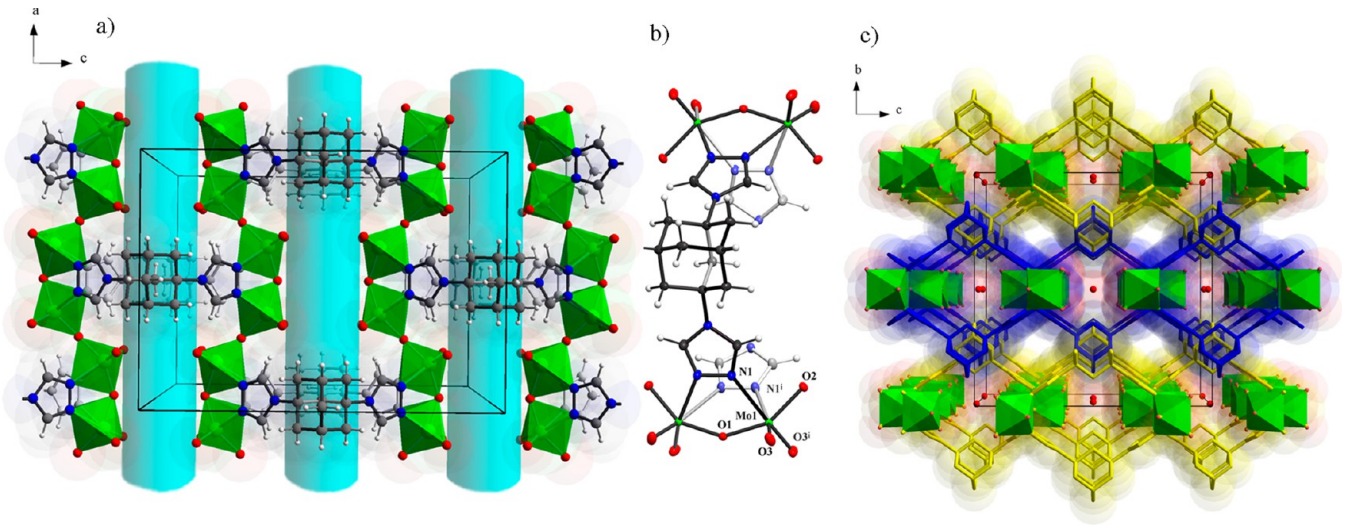

Figure 4. Formation of layered **6**·H_2O and its crystal packing (Mo shown as polyhedra). Symmetry code: (i) $x, -y, z$.

Table 2. Thermal Behavior of a Series of Samples 1−3, 4a, 5, and 6 Studied by PXRD and TGA Methods

compound	PXRD	TGA
$[MoO_3(trNH_2)]$ (**1**)	280 °C one-step decomposition[a]	ligand decomposition above 300 °C
$[Mo_2O_6(trpzH)(H_2O)_2]$ (**2**)	160−170 °C first step, 220−230 °C second step, and 290−300 °C final decompositions	7.32% water loss in the 115−220 °C range (7.39% calcd weight loss for two H_2O molecules); ligand decomposition above 300 °C
$[Mo_2O_6(m\text{-trtzH})(H_2O)_2]$ (**3**)	235 °C one-step decomposition[a]	water loss above 150 °C, followed by ligand decomposition above 240−250 °C
$[MoO_3(p\text{-trtzH})]$ (**4a**)	260 °C one-step decomposition[a]	ligand decomposition occurs above 280 °C
$[Mo_2O_6(p\text{-tr}_2Ph)]\cdot H_2O$ (**5**)	320−330 °C one-step decomposition[a]	ligand decomposition occurs above 350 °C
$[Mo_2O_6(tr_2ad)]\cdot H_2O$ (**6**)	340−350 °C one-step decomposition[a]	2.09% water loss, 115−220 °C (3.13% calcd for H_2O molecule); ligand decomposition above 370 °C

[a]No phase transformations observed.

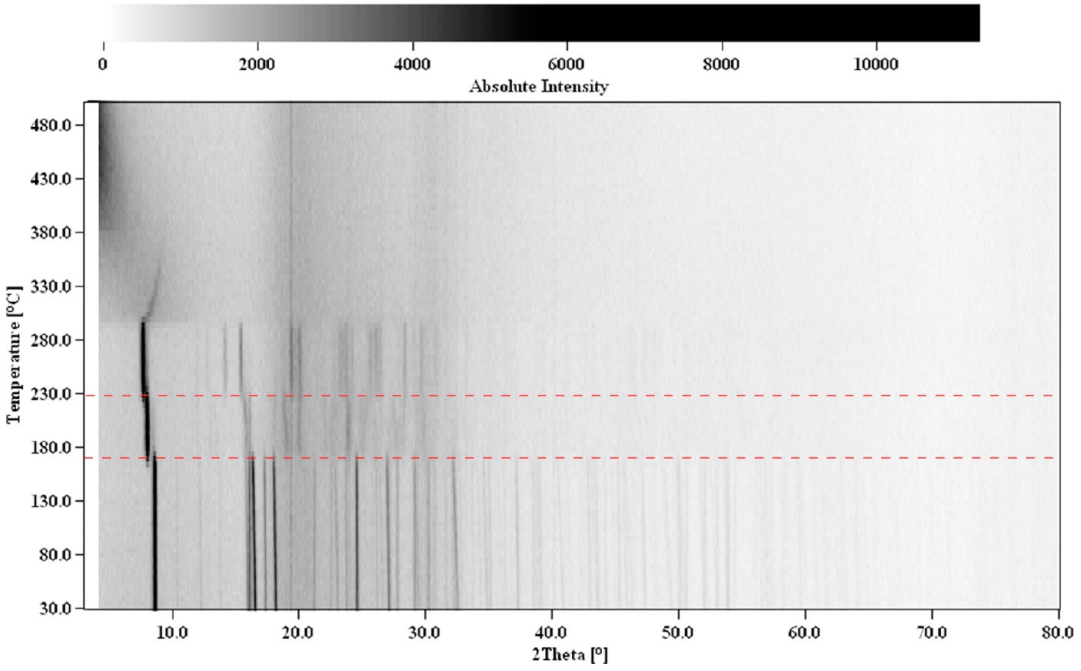

Figure 5. Thermo-PXRD pattern ($2\theta = 5-80°$) for **2**, displaying a double-stage thermal conversion (at 160−170 and 220−230 °C; dashed red lines) before the final MOOF collapse above 290 °C.

DOI: 10.1021/acs.inorgchem.5b01007
Inorg. Chem. 2015, 54, 8327−8338

are shifted in two narrow temperature intervals, 160−170 and 220−230 °C, corresponding to the first and second steps of the conversion. Apparently, the low-temperature effect can be associated with the elimination of two water molecules, while the understanding of the high-temperature structural metamorphosis is not so trivial and clear. Some important conclusions can be drawn by analyzing the organic ligand thermal degradation. Thus, the azole ligands coordinating to the molybdenum(VI) oxide matrix are essentially stable up to 235 °C (for *m*-trtzH) or even higher temperature (up to 340−350 °C for tr_2ad). The effect primarily depends on the nature of the heterocycles coupled together and the structural topological features of the MOOFs, increasing in the following order: *m*-trtzH (**3**, 1D) < *p*-trtzH (**4a**, 1D) ~ $trNH_2$ (**1**, 1D) and trpzH (**2**, 1D) < *p*-tr_2Ph (**5**, 3D) < tr_2ad (**6**, 2D). As expected, the nitrogen-rich and electron-deficient tetrazolyl derivatives (*m*-trtzH and *p*-trtzH) tend to be less stable in comparison with $trNH_2$ and trpzH ligands bearing basic moieties. Higher thermal stability for bitriazoles (*p*-tr_2Ph, **5**; tr_2ad, **6**) probably lies within the possibility of a more stable four-point coordination link that leads to stiffer 3D and 2D framework motifs.

Catalytic Epoxidation Activity of Compounds 1−6. Compounds**1−6** were tested as (pre)catalysts for epoxidation of Cy, chosen as a model substrate. The catalytic tests were carried out using a hydroperoxide oxidant, namely, TBHP or H_2O_2, at 70 °C. The catalytic performances were compared on the basis of similar initial molar ratios of Mo:Cy:oxidant = 1:100:153. Under the different reaction conditions used, 1,2-cyclooctane oxide (CyO) was always the only product formed. In the absence of molybdenum species and/or oxidant, the conversion of Cy was negligible.

The compounds tested possess catalytic activity for Cy epoxidation with TBHP. The best-performing catalyst was **2**, which led to quantitative epoxide yield at 24 h of reaction (Figure 6). For all compounds, an initial induction period of ca. 30−60 min was observed, which may be partly due to differences in the catalyst dissolution rates and solubilities.

For all catalytic systems with TBHP as the oxidant, the reaction mixtures were biphasic solid−liquid (white or off-white solids and colorless liquid phases). The undissolved solids were recovered after 24 h of reaction (see the details given in the Experimental Section) and characterized in order to check their stabilities. The PXRD patterns (Figure 7) and FT-IR ATR spectra (Figure 8) of the recovered solids were similar to the corresponding data for the original compounds. SEM images

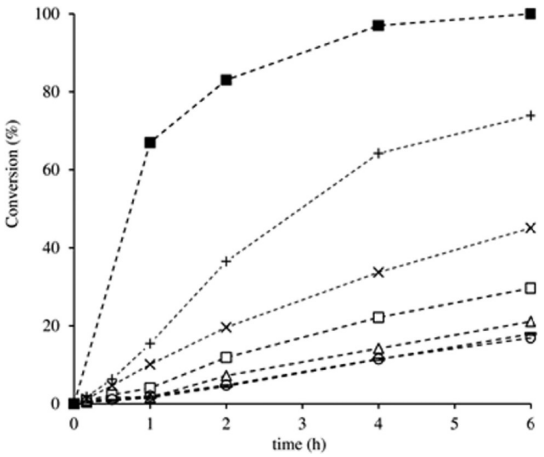

Figure 6. Cy epoxidation at 70 °C with TBHP/TFT in the presence of **1** (×), **2** (+), **3** (△), **4a** (□), **5** (○), and **6** (—) or with H_2O_2/CH_3CN in the presence of **2** (■). The dashed lines are visual guides.

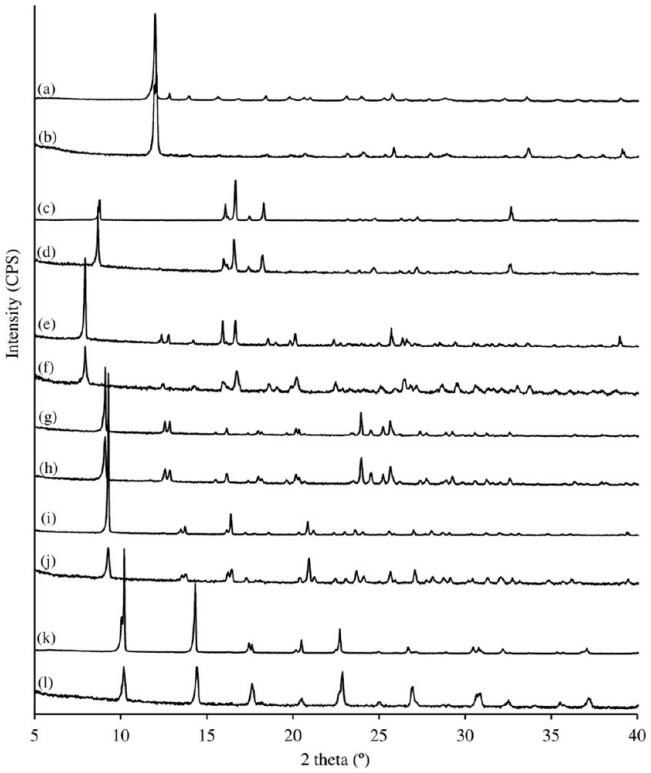

Figure 7. PXRD patterns for ***i*** and the corresponding recovered solids after 24 h of reaction with TBHP/TFT, where ***i*** = **1**(a and b), **2** (c and d), **3** (e and f), **4a** (g and h), **5** (I and j), or **6** (k and l).

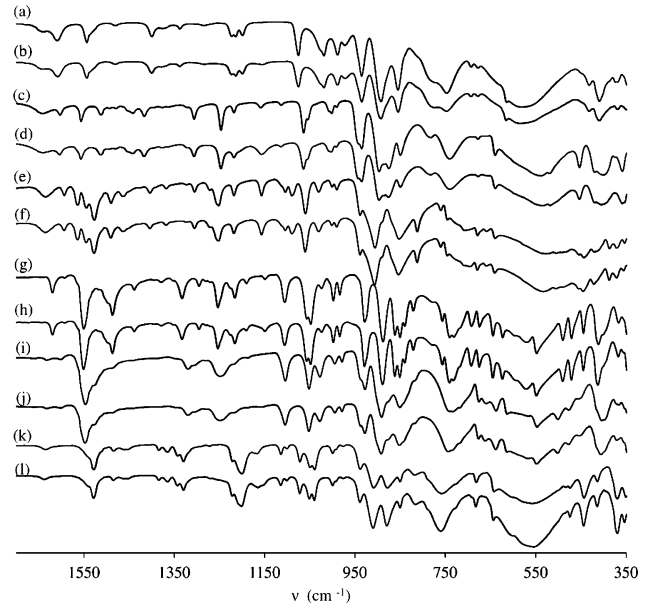

Figure 8. FT-IR ATR spectra for ***i*** and the corresponding recovered solids after 24 h of reaction with TBHP/TFT at 70 °C, where ***i*** = **1** (a and b), **2** (c and d), **3** (e and f), **4a** (g and h), **5** (I and j), and **6** (k and l).

DOI: 10.1021/acs.inorgchem.5b01007
Inorg. Chem. 2015, 54, 8327−8338

and elemental (molybdenum) mapping of the compounds before and after the catalytic reaction indicated that no drastic morphological changes occurred during catalytic reactions, and the metal dispersion remained fairly homogeneous (exemplified for **2** in Figure 9). Hence, the compounds essentially retained their structural features under the TBHP oxidizing conditions.

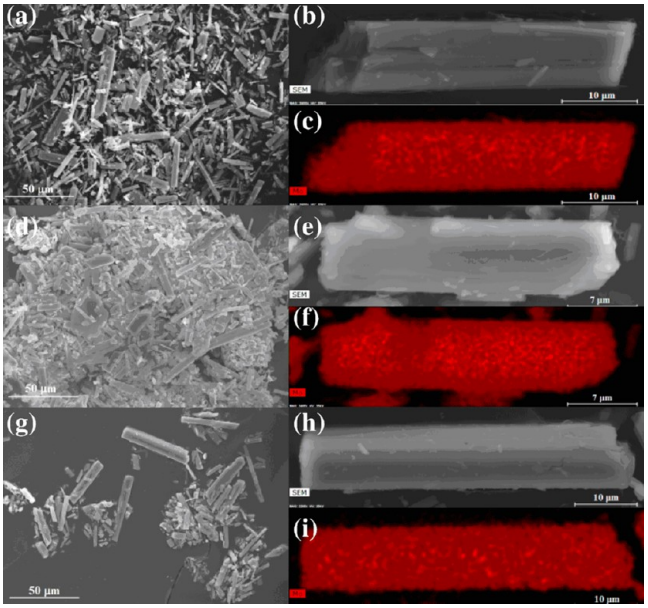

Figure 9. SEM images of **2** (a and b), the solid recovered from the catalytic reaction system Cy/TBHP/**2** (d and e), **2**-S-ct (g and h), and the corresponding molybdenum distribution maps (c, f, and i).

In order to check whether the catalytic reaction occurred in homogeneous or heterogeneous phase, a ct was carried out for **2** (without olefin; see the details given in the Experimental Section). The obtained liquid (denoted as **2**-L-ct) and solid (**2**-S-ct) phases were tested for the reaction of Cy with TBHP, at 70 °C. The catalytic tests with **2**-L-ct (homogeneous reaction mixture) and **2**-S-ct (biphasic solid−liquid) gave results similar to those with the original catalyst **2** (98−100% CyO yield at 24 h). Hence, the catalytic reaction occurs essentially in the homogeneous phase. From the catalytic test with **2**-S-ct, the solid was recovered [giving (**2**-S-ct)-run1] and characterized. Comparisons of the FT-IR ATR spectra (Figure S19) and PXRD patterns (Figure S20) of the solids (**2**-S-ct)-run1, **2**-S-ct, and **2** and of the SEM images and elemental (molybdenum) mapping of **2**-S-ct and **2** (Figure 9) indicated that the original and used catalysts possessed similar structural and chemical features. The similar characterization results correlated with the similar catalytic results for the original and used solids, and thus **2** seems to be a fairly stable catalyst.

The catalytic activities of compounds **1**−**3**, **4a**, **5**, and **6** followed the order (based on conversions at 1 h/6 h): **2** (15%/74%) > **1** (10%/45%) > **4a** (4%/30%) > **3** (2%/21%) ≅ **5** (2%/17%) ≅ **6** (2%/18%). The catalysts possessing 1D topology (**1**, **2**, and **4a**) seem to be more active than those possessing 2D or 3D topologies (**6** and **5**, respectively). The 1D topology may facilitate the accessibility of the active metal centers to the reagent molecules. However, differences in topological features do not, at least solely, explain the fact that compound **3** (1D) possessed similarly poor catalytic activity to compounds **6** and **5** (2D and 3D). On the other hand, significant differences in the catalytic activities were observed

Table 3. Comparison of the Catalytic Results for 2 to Literature Data for Molybdenum(VI) Oxide Hybrid Polymers, Tested as Catalysts for the Reaction of Cy with TBHP

	reaction conditions[b]							
compound[a]	Mo:Cy:TBHP	T (°C)	Solv	t (h)	conv[c] (%)	selectivity[d] (%)	TOF[e] (mol mol_{Mo}^{-1} h^{-1})	ref
2	1:100:153	70	TFT	6/24	74/100	100	11	
$[MoO_3(bipy)]_n$	1:100:153	55	DCE	6	95	100	68	27a
$[MoO_3(bipy)]_n$	1:100:153	75	DCE	6	100	100	518	27a
$\{[MoO_3(bipy)][MoO_3(H_2O)]\}_n$	1:100:150	55	DCE	48	62	100	n.a.	5b
$\{[MoO_3(bipy)][MoO_3(H_2O)]\}_n$	1:100:150	75	Hex	24	81	100	n.a.	5b
$\{[MoO_3(bipy)][MoO_3(H_2O)]\}_n$	1:100:150[f]	55		24	24	100	n.a.	5b
$\{[MoO_3(bipy)][MoO_3(H_2O)]\}_n$	1:100:153[f]	70	H_2O	24	38	100	n.a.	28
$[Mo_2O_6(HpypzA)]_n$	1:100:153	55	DCE	24	74	100	n.a.	5f
$[Mo_2O_6(HpypzA)]_n$	1:100:153[f]	55	EtOH	24	16	100	n.a.	5f
$[Mo_2O_6(pent\text{-}pp)]_n$	1:113:172	55	TFT	6	98	100	155	29
$[Mo_3O_9(pypz)]_n$	1:100:153	75	TFT	6/24	60/100	100	6	5c
$[PiperazinCH_2\{MoO_2(Salen)\}]_n$	1:200:200	75	DCE	12	98	n.a.	n.a.	27b
$[PiperazinCH_2\{MoO_2(Salen)\}]_n$	1:200:200[g]	75	DCE	12	95	98	n.a.	27b
$[PiperazinCH_2\{MoO_2(Salophen)\}]_n$	1:200:200[g]	75	DCE	12	89	97	n.a.	27b
$[PiperazinCH_2\{MoO_2(Salpn)\}]_n$	1:200:200[g]	75	DCE	12	93	97	n.a.	27b
$[MoO_2(L_1)]_n$	1:2000:4000[f]	80		6	72	87	484*	27c
$[MoO_2(L_2)]_n$	1:2000:4000[f]	80		6	54	87	818*	27c
$[MoO_2(L_3)]_n$	1:2000:4000[f]	80		6	23	73	530*	27c

[a]bipy = 2,2′-bipyridine; HpypzA = [3-(pyridinium-2-yl)-1*H*-pyrazol-1-yl]-acetate; pent-pp = 2-(1-pentyl-3-pyrazolyl)pyridine; pypz =2-[3(5)-pyrazolyl]pyridine; Salen = *N*,*N*′-bis(salicylidene)ethylenediamine; Salophen = *N*,*N*′-phenylenebis(salicylideneimine); Salpn = *N*,*N*′-propylenebis-(salicylideneiminato); H_2L_1 = pyridoxal isonicotinic acid hydrazone; H_2L_2 = pyridoxal benzhydrazone; H_2L_3 = pyridoxal 4-hydroxy. [b]Initial molar ratios of Mo:Cy:TBHP; T = reaction temperature; Solv = cosolvent (TFT = α,α,α-trifluorotoluene, DCE = 1,2-dichloroethane, Hex = hexane, and EtOH = ethanol); reaction time (t); n.a. = data not available/specified. [c]Conversion of Cy. [d]Selectivity to CyO. [e]TOF = turnover frequency calculated for 10 min reaction (excluding the results with *, for which the TOF was calculated for 20 min of reaction). [f]70% aqueous TBHP was used. [g]80% TBHP in di-*tert*-butyl peroxide/water (3:2) was used.

DOI: 10.1021/acs.inorgchem.5b01007
Inorg. Chem. 2015, 54, 8327−8338

Table 4. Comparison of the Catalytic Results for 2 to Literature Data for Molybdenum(VI) Oxide Hybrid Polymers, Tested as Catalysts for the Reaction of Cy with H_2O_2

	reaction conditions[b]						
compound[a]	Mo:Cy:H_2O_2	T (°C)	solvent	t (h)	conv[c] (%)	selectivity[d] (%)	ref
2	1:100:153	70	CH_3CN	4/24	97/100	100	
$\{[MoO_3(bipy)][MoO_3(H_2O)]\}_n$	1:100:153	55		48	11	100	5b
$\{[MoO_3(bipy)][MoO_3(H_2O)]\}_n$	1:100:153	70	CH_3CN	24	79	100	28
$[MoO(O_2)(4,4'\text{-bipy})]_n$	1:33:89	rt	DCM	7	~40	100	31
$[MoO_3(pdtc)]_n$	1:33:327	rt	DCM	7.5	63	100	32

[a]bipy = 2,2′-bipyridine; 4,4′-bipy = 4,4′-bipyridine; pdtc = pyrrolidine dithiocarbamate. [b]Initial molar ratios of Mo:Cy:H_2O_2; T = reaction temperature (rt = ambient temperature); Solv = cosolvent (CH_3CN = acetonitrile; DCM = dichloromethane); reaction time (t). [c]Conversion of Cy. [d]Selectivity to CyO.

for compounds possessing 1D topology and with structural similarities, namely, **2** versus **3** {general formula $[Mo_2O_6(tr)(H_2O)_2]$} and **4a** versus **1** {general formula $[MoO_3(tr)]$}. The type of organic ligand may influence the catalytic performance. It is generally accepted that molybdenum-catalyzed epoxidation of olefins occurs via heterolytic peroxometal pathways and involves an active oxidizing species that is formed via acid−base reaction between the (Lewis acid) metal center and the (base) hydroperoxide oxidant.[26] Accordingly, enhanced Lewis acidity of the metal center may lead to an improved epoxidation activity of the molybdenum catalysts. The organic ligands of compounds tested may possess different base strengths, influencing the Lewis acidity of the catalyst. For example, the ligand $trNH_2$ of **1** is likely more basic than (electron-deficient) *p*-trtzH of **4a**, which may lead to reduced Lewis acidity of **1** and consequently lower catalytic activity.

Table 3 compares the catalytic results for **2** with the literature data for other molybdenum hybrid compounds tested as catalysts in the same model reaction, i.e., Cy epoxidation with TBHP. On the basis of the conversion data for which epoxide selectivity was 100%, the catalytic results for **2** are fairly good, e.g., in relation to $\{[MoO_3(bipy)][MoO_3(H_2O)]\}_n$ (bipy = 2,2′-bipyridine),[5b] and $[Mo_3O_9(pypz)]_n$ (pypz = 2-[3(5)-pyrazolyl]pyridine).[5c] Higher conversions were reported for $[Mo_2O_6(pent\text{-}pp)]_n$[29] and $[MoO_3(bipy)]_n$.[27a] Hybrid polymeric compounds possessing salen- or hydrazone-type ligands tended to be less selective epoxidation catalysts.[27b,c] The differences in the catalytic activities may be due to a complex interplay of various factors, which may include active-site accessibility, steric and electronic effects, and catalyst solubility and stability.

Compound **2** was further investigated for Cy epoxidation using H_2O_2 as the oxidant (CH_3CN as the cosolvent). The initial epoxidation rate was significantly higher with H_2O_2 as the oxidant instead of TBHP, and the epoxide selectivity was always 100% (Table 4). These results are interesting because H_2O_2 can be considered a greener oxidant than TBHP in that the conversion of H_2O_2 gives H_2O as the coproduct (also the solvent of the oxidant solution), whereas that of TBHP conversion gives *tert*-butanol. The faster olefin epoxidation with H_2O_2 may be partly due to the enhanced catalyst solubility because compound **2** was completely soluble in the reaction mixture, whereas with TBHP as the oxidant, the reaction mixture was biphasic solid−liquid. The kinetic differences observed for the two types of oxidants may be due to differences in the reaction mechanisms. According to the literature, the epoxidation reaction with H_2O_2 may involve transfer of the O^{β} atom of an intermediate possessing the moiety $\{Mo(OH)(O^{\alpha}O^{\beta}H)\}$ to the incoming olefin substrate, with a concomitant 1,2 shift of the proton from O_{β} to O_{α}; this process is not possible in the case of TBHP, where an intermediate possessing the moiety $\{Mo(OH)(O^{\alpha}O^{\beta}tBu)\}$ is typically formed.[30]

For the catalytic system with **2**/H_2O_2, it was possible to precipitate a solid (denoted as **2***) from the liquid phase after 24 h of reaction (see the details in the Experimental Section). On the basis of the FT-IR ATR spectra of **2*** and **2**, the two solids possess comparable chemical features (Figure S19). SEM and PXRD indicated that the particle morphology and crystallinity of **2** changed during the catalytic reaction; **2*** consisted of smaller particles with amorphous structure (Figure S21). The recovered solid **2*** was tested for Cy epoxidation with H_2O_2 and led to slightly lower conversion at 24 h of reaction (82%) than **2**. After 24 h, soluble metal species (denoted as **2****) were isolated from the reaction solution; **2**** exhibited a FT-IR ATR spectrum similar to those of **2*** and **2**, suggesting that the catalyst retained its chemical features (Figure S19). The differences in the catalytic results between **2*** and **2**** may be partly due to morphological and crystalline structure modifications.

Table 4 compares the catalytic results for **2** with the literature data for other molybdenum(VI) oxide hybrids, tested as catalysts in Cy epoxidation with H_2O_2. On the basis of CyO yields at 24 h of reaction, the catalytic results for **2** are fairly good. The catalytic performances may be due to an interplay of different factors, including electronic and steric effects, catalyst solubility, and, on the other hand, some differences in the reaction conditions between different studies.

Oxidative Dehydrogenation and Aldehyde Oxidation Activity of 2. The catalytic production of substances with industrial importance from raw materials available in nature instead of substrates derived from petrochemistry is a challenge for the chemical industry. The oxidation of BzOH, which is present in a variety of essential oils (jasmine, hyacinth), can give PhCHO and benzoic acid ($PhCO_2H$). The two reaction products have wide application profiles, being used in different sectors of the chemical industry, e.g., cosmetics, perfumery, food preservation, fragrances and flavors, agrochemicals, and drugs.[33]

The catalytic performance of **2** was further investigated for the oxidative dehydrogenation of BzOH and the oxidation of PhCHO with H_2O_2, at 70 °C. The reaction of BzOH gave PhCHO and $PhCO_2H$ with 79% and 21% selectivity, respectively, at 53% BzOH conversion, in 24 h; without catalyst, conversion was 7%. According to the literature, the oxidation of BzOH to PhCHO with H_2O_2 may be promoted by intermediate peroxomolybdenum species.[34] The oxidation of PhCHO in the presence of **2** gave $PhCO_2H$ with 100%

DOI: 10.1021/acs.inorgchem.5b01007
Inorg. Chem. 2015, 54, 8327−8338

selectivity, at 58% conversion, in 24 h; without catalyst, conversion was 6%. To the best of our knowledge, this is the first report of the oxidation of BzOH or PhCHO with H_2O_2 in the presence of a molybdenum(VI) oxide hybrid.

CONCLUSION

In this work, we employed the specially designed 1,2,4-triazole ligands for the rational construction of molybdenum(VI) oxide hybrid solids. The organic ligands are tethered to Mo centers through two [N−N]-triazole donor sites. The secondary groups like amine, pyrazole, or 1*H*-tetrazole behave as H-donor/acceptor modules for hydrogen-bonding interactions that support the formation of chain, ribbon, or helix topologies. The presence of two triazole functions leads to rigid 2D and 3D frameworks. The prepared complexes exhibit enhanced thermal stability. The molybdenum(VI) oxide compounds possess olefin epoxidation activity, demonstrated by the model reaction of Cy using TBHP or aqueous H_2O_2 as an oxygen source. The catalysts possessing 1D structures (**1**, **2**, and **4a**) were more active than those possessing 2D or 3D topologies (**6** and **5**, respectively). In turn, the presence of the coordinated organic ligands with different acidic−basic and steric properties allowed a fine-tuning of the catalytic activity at the molecular level. Superior catalytic performance was observed for **2**. This molybdenum(VI) oxide hybrid was successfully explored as a versatile catalyst in the oxidative dehydrogenation of BzOH with H_2O_2 and the oxidation of PhCHO to $PhCO_2H$.

ASSOCIATED CONTENT

Supporting Information

The Supporting Information is available free of charge on the ACS Publications website at DOI: 10.1021/acs.inorgchem.5b01007.

Experimental details for X-ray structural analyses, spectral characterization data, thermal PXRD patterns, and DTA/TG−MS data (PDF)

Crystallographic data, (CIF)

AUTHOR INFORMATION

Corresponding Authors

*E-mail: ab_lysenko@univ.kiev.ua (L.A.B.).

*E-mail: igoncalves@ua.pt (I.S.G.).

Notes

The authors declare no competing financial interest.

ACKNOWLEDGMENTS

Financial support by Deutsche Forschungsgemeinschaft is gratefully acknowledged. The Portuguese (PT) group acknowledge funding by FEDER (Fundo Europeu de Desenvolvimento Regional) through COMPETE (Programa Operacional Factores de Competitividade). National PT funding through the FCT (Fundação para a Ciência e a Tecnologia) within Project FCOMP-01-0124-FEDER-029779 (FCT ref PTDC/QEQ-SUP/1906/2012) is thanked. This work (PT) was partly developed in the scope of the project CICECO - Aveiro Institute of Materials (FCT ref UID/CTM/50011/2013), financed by national funds through the FCT/MEC and cofinanced by FEDER under the PT2020 Partnership Agreement. The FCT and EU are acknowledged for a postdoctoral grant to P.N. (SFRH/BPD/73540/2010) cofunded by MCTES and the European Social Fund through the program POPH of QREN.

REFERENCES

(1) (a) Miras, H. N.; Vilà-Nadal, L.; Cronin, L. *Chem. Soc. Rev.* **2014**, *43*, 5679−5699. (b) Miras, H. N.; Yan, J.; Long, D.-L.; Cronin, L. *Chem. Soc. Rev.* **2012**, *41*, 7403−7430. (c) Dolbecq, A.; Dumas, E.; Mayer, C. R.; Mialane, P. *Chem. Rev.* **2010**, *110*, 6009−6048. (d) *New Strategies in Chemical Synthesis and Catalysis*; Pignataro, B., Eds.; Wiley-VCH: Weinheim, Germany, 2012.

(2) Xia, Q.-H.; Ge, H.-Q.; Ye, C.-P.; Liu, Z.-M.; Su, K.-X. *Chem. Rev.* **2005**, *105*, 1603−1662.

(3) (a) Lorret, O.; Lafond, V.; Mutin, P. H.; Vioux, A. *Chem. Mater.* **2006**, *18*, 4707−4709. (b) Coles, M. P.; Lugmair, C. G.; Terry, K. W.; Tilley, T. D. *Chem. Mater.* **2000**, *12*, 122−131. (c) Wu, P.; Tatsumi, T. *Chem. Commun.* **2002**, *14*, 1026−1027. (d) Xu, L.; Sithambaram, S.; Zhang, Y.; Chen, C.-H.; Jin, L.; Joesten, R.; Suib, S. L. *Chem. Mater.* **2009**, *21*, 1253−1259. (e) Yang, X.-L.; Wu, C.-D. *Inorg. Chem.* **2014**, *53*, 4797−4799. (f) Muratsugu, S.; Weng, Z.; Tada, M. *ACS Catal.* **2013**, *3*, 2020−2030. (g) Cheng, L.; Yin, C.; Mehmood, F.; Liu, B.; Greeley, J.; Lee, S.; Lee, B.; Seifert, S.; Winans, R. E.; Teschner, D.; Schlögl, R.; Vajda, S.; Curtiss, L. A. *ACS Catal.* **2014**, *4*, 32−39. (h) Tada, M.; Muratsugu, S.; Kinoshita, M.; Sasaki, T.; Iwasawa, Y. *J. Am. Chem. Soc.* **2010**, *132*, 713−724. (i) Mello, R.; Alcalde-Aragonés, A.; González Núñez, M. E.; Asensio, G. *J. Org. Chem.* **2012**, *77*, 6409−6413. (j) Song, F.; Wang, C.; Falkowski, J. M.; Ma, L.; Lin, W. *J. Am. Chem. Soc.* **2010**, *132*, 15390−15398.

(4) (a) Muñoz-Espí, R.; Burger, C.; Krishnan, C. V.; Chu, B. *Chem. Mater.* **2008**, *20*, 7301−7311. (b) Barrio, L.; Campos-Martín, J. M.; de Frutos, M. P.; Fierro, J. L. G. *Ind. Eng. Chem. Res.* **2008**, *47*, 8016−8024.

(5) (a) Du, J.; Yu, J.; Tang, J.; Wang, J.; Zhang, W.; Thiel, W. R.; Jia, M. *Eur. J. Inorg. Chem.* **2011**, *2011*, 2361−2365. (b) Abrantes, M.; Amarante, T. R.; Antunes, M. M.; Gago, S.; Almeida Paz, F. A.; Margiolaki, I.; Rodrigues, A. E.; Pillinger, M.; Valente, A. A.; Gonçalves, I. S. *Inorg. Chem.* **2010**, *49*, 6865−6873. (c) Amarante, T. R.; Neves, P.; Gomes, A. C.; Nolasco, M. M.; Ribeiro-Claro, P.; Coelho, A. C.; Valente, A. A.; Paz, F. A. A.; Smeets, S.; McCusker, L. B.; Pillinger, M.; Gonçalves, I. S. *Inorg. Chem.* **2014**, *53*, 2652−2665. (d) Amarante, T. R.; Neves, P.; Valente, A. A.; Almeida Paz, F. A.; Fitch, A. N.; Pillinger, M.; Gonçalves, I. S. *Inorg. Chem.* **2013**, *52*, 4618−4628. (e) Amarante, T. R.; Neves, P.; Tomé, C.; Abrantes, M.; Valente, A. A.; Paz, F. A. A.; Pillinger, M.; Gonçalves, I. S. *Inorg. Chem.* **2012**, *51*, 3666−3676. (f) Figueiredo, S.; Gomes, A. C.; Neves, P.; Amarante, T. R.; Almeida Paz, F. A.; Soares, R.; Lopes, A. D.; Valente, A. A.; Pillinger, M.; Gonçalves, I. S. *Inorg. Chem.* **2012**, *51*, 8629−8635.

(6) (a) Jia, M.; Seifert, A.; Thiel, W. R. *Chem. Mater.* **2003**, *15*, 2174−2180. (b) Jia, M.; Seifert, A.; Berger, M.; Giegengack, H.; Schulze, S.; Thiel, W. R. *Chem. Mater.* **2004**, *16*, 877−882.

(7) Zhang, X.; Hejazi, M.; Thiagarajan, S. J.; Woerner, W. R.; Banerjee, D.; Emge, T. J.; Xu, W.; Teat, S. J.; Gong, Q.; Safari, A.; Yang, R.; Parise, J. B.; Li, J. *J. Am. Chem. Soc.* **2013**, *135*, 17401−17407.

(8) 2,2′-bipy: (a) Zapf, P. J.; Haushalter, R. C.; Zubieta, J. *Chem. Mater.* **1997**, *9*, 2019−2023. (b) Yan, B.; Xu, Y.; Goh, N. K.; Chia, L. S. *Inorg. Chem. Commun.* **2000**, *3*, 379−382. (c) Kim, J.; Lim, W. T.; Koo, B. K. *Inorg. Chim. Acta* **2007**, *360*, 2187−2191.

(9) 1,10-phen: (a) Zhou, D. P.; Bi, D. Q. *Z. Kristallogr. New Cryst. Struct.* **2006**, *221*, 503−504. (b) Zhao, B.; Chen, X. Y.; Cheng, P.; Ding, B.; Liao, D. Z.; Yan, S. P.; Jiang, Z. H. *J. Coord. Chem.* **2005**, *58*, 467−472.

(10) en: Yang, S.; Li, G.; Tian, S.; Liao, F.; Lin, J. *Cryst. Growth Des.* **2007**, *7*, 1246−1250.

(11) Johnson, J. W.; Jacobson, A. J.; Rich, S. M.; Brody, J. F. *J. Am. Chem. Soc.* **1981**, *103*, 5246−5247.

(12) (a) Yan, B.; Xu, Y.; Goh, N. K.; Chia, L. S. *Chem. Commun.* **2000**, 2169−2170. (b) Hagrman, P. J.; LaDuca, R. L., Jr.; Koo, H. J.; Rarig, R., Jr.; Haushalter, R. C.; Whangbo, M. H.; Zubieta, J. *Inorg. Chem.* **2000**, *39*, 4311−4317.

(13) (a) Xu, Y.; Lu, J.; Goh, N. K. *J. Mater. Chem.* **1999**, *9*, 1599−1602. (b) Pang, S.; Jian, F.; Wang, L. *Inorg. Chem.* **2008**, *47*, 344−348.

(14) Chuang, J.; Ouellette, W.; Zubieta, J. *Inorg. Chim. Acta* **2008**, *361*, 2357−2364.

DOI: 10.1021/acs.inorgchem.5b01007
Inorg. Chem. 2015, 54, 8327−8338

(15) Lysenko, A. B.; Senchyk, G. A.; Lincke, J.; Lässig, D.; Fokin, A. A.; Butova, E. D.; Schreiner, P. R.; Krautscheid, H.; Domasevitch, K. V. *Dalton Trans.* **2010**, *39*, 4223−4231.
(16) (a) *X-SHAPE*, revision 1.06; Stoe & Cie GmbH: Darmstadt, Germany, 1999. (b) *X-RED*, version 1.22; Stoe & Cie GmbH: Darmstadt, Germany, 2001.
(17) (a) Sheldrick, G. M. *SHELX97, A system of computer programs for X-ray structure determination*; University of Göttingen: Göttingen, Germany, 1997. (b) Sheldrick, G. M. *Acta Crystallogr., Sect. A: Found. Crystallogr.* **1990**, *46*, 467−473.
(18) *IPDS Software*; Stoe & Cie GmbH: Darmstadt, Germany, 2000.
(19) Brandenburg, K. *Diamond 2.1e*; Crystal Impact GbR: Bonn, 1999.
(20) (a) Govor, E. V.; Lysenko, A. B.; Quinõnero, D.; Rusanov, E. B.; Chernega, A. N.; Moellmer, J.; Staudt, R.; Krautscheid, H.; Frontera, A.; Domasevitch, K. V. *Chem. Commun.* **2011**, *47*, 1764−1766. (b) Bondar, O. A.; Lukashuk, L. V.; Lysenko, A. B.; Krautscheid, H.; Rusanov, E. B.; Chernega, A. N.; Domasevitch, K. V. *CrystEngComm* **2008**, *10*, 1216−1226. (c) Senchyk, G. A.; Lysenko, A. B.; Rusanov, E. B.; Chernega, A. N.; Krautscheid, H.; Domasevitch, K. V. *Inorg. Chim. Acta* **2009**, *362*, 4439−4448.
(21) Li, S.; Zhou, Z.; Zhang, Y.; Liu, M.; Li, W. *Chem. Mater.* **2005**, *17*, 5884−5886.
(22) Sharga, O. V.; Lysenko, A. B.; Handke, M.; Krautscheid, H.; Rusanov, E. B.; Chernega, A. N.; Krämer, K. W.; Liu, S.-X.; Decurtins, S.; Bridgeman, A.; Domasevitch, K. V. *Inorg. Chem.* **2013**, *52*, 8784−8794.
(23) Chen, S.-M.; Lu, C.-Z.; Yu, Y.-Q.; Zhang, Q.-Z.; He, X. *Acta Crystallogr., Sect. C: Cryst. Struct. Commun.* **2004**, *60*, m437−m439.
(24) Lässig, D.; Lincke, J.; Gerhardt, R.; Krautscheid, H. *Inorg. Chem.* **2012**, *51*, 6180−6189.
(25) Vasylevs'kyy, S. I.; Senchyk, G. A.; Lysenko, A. B.; Rusanov, E. B.; Chernega, A. N.; Jezierska, J.; Krautscheid, H.; Domasevitch, K. V.; Ozarowski, A. *Inorg. Chem.* **2014**, *53*, 3642−3654.
(26) (a) Comas-Vives, A.; Lledos, A.; Poli, R. *Chem. - Eur. J.* **2010**, *16*, 2147−2158. (b) Al-Ajlouni, A.; Valente, A. A.; Nunes, C. D.; Pillinger, M.; Santos, A. M.; Zhao, J.; Romão, C. C.; Gonçalves, I. S.; Kühn, F. E. *Eur. J. Inorg. Chem.* **2005**, *2005*, 1716−1723. (c) Calhorda, M. J.; Costa, P. J. *Curr. Org. Chem.* **2012**, *16*, 65−72. (d) Nunes, C. D.; Calhorda, M. J. *Inorg. Chim. Acta* **2015**, *431*, 122−131. (e) Grover, N.; Drees, M.; Kühn, F. E. *J. Catal.* **2015**, *329*, 269−285.
(27) (a) Amarante, T. R.; Neves, P.; Coelho, A. C.; Gago, S.; Valente, A. A.; Paz, F. A. A.; Pillinger, M.; Gonçalves, I. S. *Organometallics* **2010**, *29*, 883−892. (b) Bagherzadeh, M.; Zare, M. *J. Coord. Chem.* **2013**, *66*, 2885−2900. (c) Pisk, J.; Prugovečki, B.; Matković-Čalogović, D.; Jednačak, T.; Novak, P.; Agustin, D.; Vrdoljak, V. *RSC Adv.* **2014**, *4*, 39000−39010.
(28) Gamelas, C. A.; Gomes, A. C.; Bruno, S. M.; Paz, F. A. A.; Valente, A. A.; Pillinger, M.; Romão, C. C.; Gonçalves, I. S. *Dalton Trans.* **2012**, *41*, 3474−3484.
(29) Amarante, T. R.; Neves, P.; Almeida Paz, F. A.; Valente, A. A.; Pillinger, M.; Gonçalves, I. S. *Dalton Trans.* **2014**, *43*, 6059−6069.
(30) (a) Dinoi, C.; Ciclosi, M.; Manoury, E.; Maron, L.; Perrin, L.; Poli, R. *Chem. - Eur. J.* **2010**, *16*, 9572−9584. (b) Dinoi, C.; Poli, R.; Perrin, L.; Maron, L. *Dalton Trans.* **2012**, *41*, 1131−1133.
(31) Afsharpour, M.; Mahjoub, A. R.; Amini, M. M. *Appl. Catal., A* **2007**, *327*, 205−2010.
(32) Afsharpour, M.; Mahjoub, A.; Amini, M. M. *J. Inorg. Organomet. Polym. Mater.* **2008**, *18*, 472−476.
(33) (a) Sharma, R. V.; Soni, K. K.; Dalai, A. K. *Catal. Commun.* **2012**, *29*, 87−91. (b) Jia, L.; Zhang, S.; Gu, F.; Ping, Y.; Guo, X.; Zhong, Z.; Su, F. *Microporous Mesoporous Mater.* **2012**, *149*, 158−165. (c) Behera, G. C.; Parida, K. M. *Appl. Catal., A* **2012**, *413-414*, 245−253. (d) Brul, S.; Coote, P. *Int. J. Food Microbiol.* **1999**, *50*, 1−17.
(34) (a) Maiti, S. K.; Malik, K. M. A.; Bhattacharyya, R. *Inorg. Chem. Commun.* **2004**, *7*, 823−828. (b) Biradar, A. V.; Dongare, M. K.; Umbarkar, S. B. *Tetrahedron Lett.* **2009**, *50*, 2885−2888.

DOI: 10.1021/acs.inorgchem.5b01007
Inorg. Chem. 2015, 54, 8327−8338